Power measurements based on the Conservative Power Theory with a reduced sampling rate for lowering implementation cost

Victor A. de A. Prado[1], Nicholas D. Andrade[1], Ianca M. S. de Jesus[1], *Member, IEEE,* Ruben B. Godoy[1], Edson A. Batista[1], and Moacyr A. G. de Brito[1], *Member, IEEE*

[1]Faculty of Engineering, Architecture and Urbanism and Geography,
Federal University of Mato Grosso do Sul - UFMS,
Av. Costa e Silva, s/nº, Campo Grande, MS, 79070-900, Brazil

***Abstract*—This paper presents an innovative approach to digitally implement the Conservative Power Theory (CPT) with a reduced sampling rate. The algorithms employed for discrete power calculations of such modern power theory operate at a sampling rate lower than 300 Hz. To enable the use of low sampling rates while maintaining acceptable accuracy and precision, various sampling scenarios were evaluated, and a data acquisition strategy was developed. Computer simulations conducted at an 8 kHz sampling rate revealed that the errors in power calculations were below 5% when compared to an idealized continuous-time (infinite sampling rate) reference. These results motivated the identification of sampling rates below 300 Hz capable of yielding comparable performance. In addition to active and reactive power, the analysis included non-conventional power quantities, taking into account unbalanced load conditions and waveform distortions. Simulations were performed using the CPT in the discrete-time domain for both unbalanced RL three-phase circuits and unbalanced nonlinear three-phase circuits. Subsequently, hypothesis testing was employed to validate the accuracy and precision of the power calculations at sampling rates below 300 Hz. Among power measurements, mean percentage errors were below 10% in 84.6% of the cases and below 2% in 61.5% of the cases. Hence, a significant reduction in the computational cost of CPT-based power calculations is achieved, enabling the proposed methodology to be implemented on low-cost, low-power microcontrollers without compromising measurement accuracy or precision.**

***Index Terms*—Conservative Power Theory, Harmonics, Reduced Computational Cost, Reduced Sample Rate.**

I. Introduction

ALTHOUGH the concepts of active power and current were established as early as the 1930s, the definitions of reactive power and power components associated with harmonic distortion remain subjects of ongoing debate (1; 2).

Active power is based on the physical phenomena of electrical power. This power can be transferred to thermal power and can be measured in thermal or mechanical forms and quantified using corresponding units. As such, its definition is well accepted for both sinusoidal and non-sinusoidal waveforms. Reactive power, while clearly defined under sinusoidal conditions, lacks a universally accepted definition in the presence of waveform distortion. Various power theories have been proposed to address this gap, introducing additional components to account for the effects of harmonic voltages and currents (3).

Non-linear loads, which are sources of harmonic distortion, adversely affect power quality in electrical systems. These harmonics increase conductor and transformer losses due to eddy currents, may cause resonances, and induce non-linear voltage drops that impact the performance of sensitive electronic devices (4).

Concurrently, the proliferation of non-linear loads and the rapid integration of distributed energy resources, such as photovoltaic systems and power converters for electric mobility, have introduced new challenges (5; 6). These include grid unbalance and frequency deviations, especially under intermittent generation conditions. In this context, accurate definition and measurement of power components, according to a consistent power theory, are essential to enable appropriate compensation strategies, such as active filtering techniques (7), and to ensure accurate energy billing.

Achieving high precision in power measurements requires higher sampling rates in order to perform accurate calculations involving RMS and average values. However, at lower sampling rates, errors in reactive and new portions of power introduced by modern power theories are unacceptable and make the CPT implementation unfeasible on low-cost microprocessors (8).

Thus, a trade-off must be established between measurement precision and computational cost, depending on application-specific requirements. In this study, a sampling rate of 8 kHz, considering a 60 Hz cycle, is considered sufficient to approximate continuous-time results with acceptable accuracy for CPT-based calculations.

The proposed methodology enables the use of the 133 samples, acquired within a 60 Hz cycle, or slightly fewer, at sampling rates below 300 Hz. Although this reduces synchronization with the signal's fundamental period, simulation results show that comparable accuracy and precision can still be achieved. This approach supports the implementation of CPT-based power measurement schemes on resource-constrained embedded platforms without compromising reliability.

A. Methods

1) Theoretical background of modern power theories: In general, modern power theories redefine reactive power and introduce additional power components to account for non-sinusoidal operating conditions. Among these theories, the Conservative Power Theory (CPT) stands out by proposing power terms with physical interpretation. Consequently, its adoption has been increasing significantly.

2) Conservative Power Theory — CPT: The Conservative Power Theory (CPT) is grounded in Tellegen's Theorem. It establishes that, for a set of branches in an electrical network where voltages and currents satisfy Kirchhoff's Voltage and Current Laws, the dot product between the voltage and current branch vectors is equal to zero. This dot product represents the total power, and since the result is zero, the power is considered conservative. Moreover, since active power is defined as the average value of the instantaneous product of voltage and current, it also exhibits conservative behavior (9).

According to Kirchhoff's Voltage Law (KVL), the sum of voltages across all branches in a closed loop is zero. Consequently, the sum of the time-integrated voltage (with zero mean) across these branches is also zero. When this unbiased time voltage integral is multiplied by the corresponding current, the result is reactive energy, which also sums to zero in a conservative system. Therefore, reactive energy is likewise considered conservative under CPT (9).

In the context of CPT, it is essential to understand the mathematical operators involved in defining the power components. These operators are formalized as scalar quantities and are presented in equations (1) to (7).

$$average\ value : \overline{x} = \frac{1}{T}\int_0^T x(t)dt \tag{1}$$

$$time\ derivative : \dot{x} = \frac{dx}{dt} \tag{2}$$

$$time\ integral : x_{\int} = \int_0^T x(\tau)dt \tag{3}$$

$$unbiased\ time\ integral : \hat{x} = x_{\int} - \overline{x}_{\int} \tag{4}$$

$$internal\ product : \langle x, y\rangle = \frac{1}{T}\int_0^T x \times y\ dt \tag{5}$$

$$norm\ (RMS\ value) : X = \|x\| = \sqrt{\langle x, x\rangle} \tag{6}$$

$$orthogonality : \langle x, y\rangle = 0 \tag{7}$$

For the case in which the variables **x** and *y* are vectors of **N** elements, equations (8) to (12) are applied. Underlined terms represent vectors.

$$dot\ product : \underline{x} \circ \underline{y} = \sum_{n=1}^{N} x_n \times y_n \tag{8}$$

$$magnitude : |\underline{x}| = \sqrt{\underline{x} \circ \underline{x}} = \sqrt{\sum_{n=1}^{N} x_n^2} \tag{9}$$

$$internal\ product : \langle \underline{x}, \underline{y}\rangle = \sum_{n=1}^{N} \langle x_n, y_n\rangle \tag{10}$$

$$norm\ (RMS\ value) : X = \|\underline{x}\| = \sqrt{\sum_{n=1}^{N} \langle x_n, x_n\rangle} \tag{11}$$

$$orthogonality : \langle \underline{x}, \underline{y}\rangle = 0 \tag{12}$$

Based on these definitions, it is possible to derive the expressions for the power and energy components defined by the Conservative Power Theory (CPT). The active power, reactive energy, and apparent power are presented in equations (13) to (15). The elements u and i are the instantaneous voltage and instantaneous current, respectively.

$$P = \overline{p} = \langle u, i\rangle \tag{13}$$

$$W = \overline{w} = \langle \hat{u}, i\rangle = -\langle u, \hat{i}\rangle \tag{14}$$

$$A = \|u\| \times \|i\| = U \times I \tag{15}$$

For polyphase systems, the active, reactive, and void components of electrical currents are defined, phase by phase, through (16) to (18). G_n denotes the phase conductance [Ohm^{-1}]. B_n represents the equivalent phase reactivity [Henry^{-}1], and n represents the phase.

$$i_{an} = \frac{\langle u_n, i_n\rangle}{\|u_n\|^2} u_n = \frac{P_n}{U_n^2} u_n = G_n \times u_n \tag{16}$$

$$i_{rn} = \frac{\langle \hat{u_n}, i_n\rangle}{\|\hat{u}_n\|^2} \hat{u}_n = \frac{W_n}{\hat{U}_n^2} \hat{u}_n = B_n \times \hat{u}_n \tag{17}$$

$$i_{vn} = i_n - i_{an} - i_{rn} \tag{18}$$

The active (i_a) and reactive currents (i_r) can be calculated collectively, by supposing a hypothetical balanced load that consumes the same active power and reactive energy that the real load consumes. These collective values of current can be decomposed into balanced (i^b) and unbalanced terms (i^u). The balanced ones are described in (19) and (20).

$$\underline{i_a^b} = \frac{\langle \underline{u}, \underline{i}\rangle}{\|\underline{u}\|^2} \underline{u} = \frac{P}{U^2} \underline{u} = G^b \times \underline{u} \tag{19}$$

$$\underline{i_r^b} = \frac{\langle \underline{\hat{u}}, \underline{i}\rangle}{\|\underline{\hat{u}}\|^2} \underline{\hat{u}} = \frac{W}{\hat{U}^2} \underline{\hat{u}} = B^b \times \underline{\hat{u}} \tag{20}$$

The unbalanced active (i_a^u) and reactive current (i_r^u) terms are described, respectively, in (21) and (22).

$$\underline{i_a^u} = \underline{i_a} - \underline{i_a^b} \tag{21}$$

$$\underline{i_r^u} = \underline{i_r} - \underline{i_r^b} \tag{22}$$

With all current terms determined, each power component of CPT can be calculated. Active and reactive power, P and Q, are, respectively, defined in (23) and (24).

$$P = U \times I_a^b = \|\underline{u}\| \times \|\underline{i_a^b}\| \tag{23}$$

$$Q = U \times I_r^b = \|\underline{u}\| \times \|\underline{i_r^b}\| \tag{24}$$

The unbalanced active power N_a, and unbalanced reactive power N_r are described in (25) and (26), respectively.

$$N_a = U \times I_a^d = \|u\| \times \|i_a^d\| = U\sqrt{\sum_{n=1}^{N} \frac{P_n^2}{U_n^2} - \frac{P^2}{U^2}} \quad (25)$$

$$N_r = U \times I_r^d = \|u\| \times \|i_r^d\| = U\sqrt{\sum_{n=1}^{N} \frac{W_n^2}{U_n^2} - \frac{W^2}{U^2}} \quad (26)$$

The unbalanced power, N, is presented in (27).

$$N = U \times I^d = \|\underline{u}\| \times \|\underline{i^d}\| = \sqrt{N_a^2 + N_r^2} \quad (27)$$

The void power is defined in (28).

$$V = U \times I_v = \|\underline{u}\| \times \|\underline{i_v}\| = \|\underline{u}\| \times \|\underline{i_a} - \underline{i_r}\| \quad (28)$$

B. Computer simulations

Computer simulations were conducted in discrete domain by sampling voltage and current waveforms, with different sampling rates: 15.36 kHz, 7.68 kHz, 1.92 kHz, 300 Hz, and 297.766779 Hz. The latter was chosen to obtain a sampling rate lower than 300 Hz, while still maintaining acceptable accuracy when compared to a reference simulation in a continuous domain.

Basic arithmetic operations—addition, subtraction, multiplication, and division—were used to calculate both average and RMS values. Specific algorithms were developed for this purpose.

The algorithms used an amount of n samples to calculate average and RMS values within a 60 Hz cycle. This quantity was obtained by dividing the sample frequencies by the 60 Hz fundamental frequency. Therefore, the algorithm for a 15.36 kHz frequency utilizes 256 samples and 7.68 kHz, 1.92 kHz and 300 Hz utilize 128, 32 and 5 samples, respectively. The calculation of the number of samples for 297.766779 Hz was described in item I-B2.

1) Average and RMS value calculations: To calculate the average value, a vector was created to store the sampled points of the waveform. These points were summed and divided by its total amount.

The RMS value algorithm was derived from mathematical operators, specifically average value, internal product, and norm (RMS value) as described in (1), (5) and (6), respectively. The key distinction between the average value and the inner product lies in the presence of the multiplication by the variable. The RMS value, in turn, is obtained as the square root of the inner product.

From the analysis of equation (1), if the x variable is squared, the same procedure used for average value calculation can be used, and in the result a square root operation is performed to obtain the RMS value.

Fig. 1. a) Sampling rate at 300 Hz. b) Sampling rate at 297.766779 Hz.

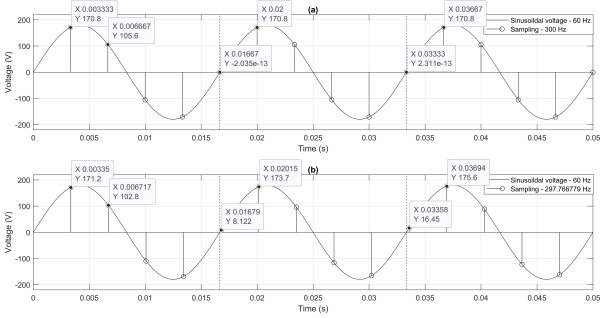

2) Reduced sampling rate: A reduced sampling rate was selected aiming for a value close to 300 Hz, as lower rates reduce computational costs. Nonetheless, the accuracy should be acceptable.

After several simulations, it was observed that an 8 kHz sampling rate, acquiring 133 samples in a 60 Hz cycle, produced errors lower than 5% in most of power measurements when compared to the reference simulation in continuous domain. So, it was defined that the sampling rate used in this project should acquire a similar number of samples to do the calculations.

Nevertheless, a 300 Hz frequency acquires only 5 samples in a 60 Hz cycle, which is insufficient for accurate power calculation. To overcome this limitation, a strategy was implemented in which samples were collected over multiple consecutive cycles until a total of 133 samples was stored in the vector. Additionally, the chosen sampling frequency could not be an integer multiple of 60 Hz; otherwise, the same sample points would be repeated in each cycle, resulting in redundant data.

Figure 1.a) illustrates a 60 Hz sinusoidal waveform sampled at a 300 Hz rate. In contrast, in Figure 1.b) the samples were obtained with a non-multiple of 60 Hz. It is seen that at each cycle, the samples with 300 Hz result in the same values, whilst with the 297.766779 Hz sampling, at each cycle, the values measured differ from the previous ones. This way, it is possible to obtain enough wave information after storing it from subsequent cycles, to form a vector that has a number of samples that leads to good accuracy for power calculation.

Hence, it was defined that the reduced sampling rate should introduce a delay among samples of subsequent cycles, corresponding to the period of an 8 kHz signal. This approach ensures that the same 133 distinct sampling points—originally captured within a single cycle at 8 kHz—are progressively acquired over multiple cycles.

The reduced sampling rate, required to obtain the desired number of points, was determined using (29) and (30).

$$n = i.d \quad (29)$$

Where:

n: number of samples at a 60 Hz cycle.

i: integer part.

d: fractional part.

As the sampling rate should be lower than 300 Hz, i was defined as 4 because 300 Hz samples 5 points in a 60 Hz cycle.

Fig. 2. a) Illustration of how the delay on the reduced sampling works. b) Zoom in the sample during the delay process.

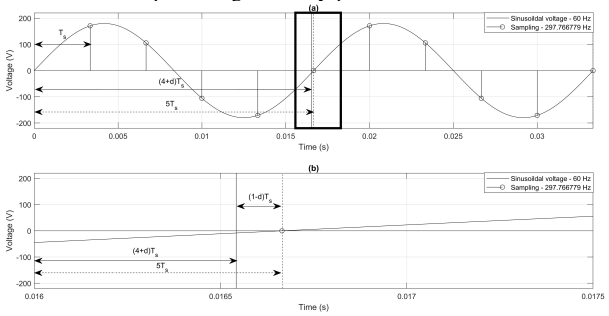

Figure 2.a) illustrates sampling at reduced rate and Figure 2.b) zooms into the black rectangle of Figure 2.a), indicating how (30) is used.

To ensure that the sampling rate remained below 300 Hz, the parameter i was set to 4, since a 300 Hz sampling rate yields 5 points in a 60 Hz cycle. Figure 2.a) illustrates the waveform sampling at the reduced rate, while Figure 2.b) presents a zoomed view of the highlighted region (black rectangle) from Figure 1.a, demonstrating the application of equation (30).

$$\begin{aligned}(1-d)T_s = a &= 1.25\times10^{-4}\\ (1-d) &= \frac{1.25\times10^{-4}}{T_s}\\ d &= 1-\frac{1.25\times10^{-4}}{T_s}\end{aligned} \tag{30}$$

Where:

a: delay between samples of two subsequent periods (period of an 8 kHz frequency). As previously discussed, this sampling frequency was selected because it yields reduced errors when compared to the reference simulation performed in the continuous-time domain.

T_s: Period of reduced sampling frequency.

From (29), n is converted to (31).

$$n = i + d = 4 + d \tag{31}$$

Moreover, n corresponds to (32).

$$n = \frac{T_r}{T_s} \tag{32}$$

Where:

T_r: period of 60 Hz cycle.

Therefore, since (32) equals (31), (33) is derived. Subsequently, by substituting (30), one can obtain (34).

$$\frac{T_r}{T_s} = 4 + d \tag{33}$$

$$\begin{aligned}\frac{T_r}{T_s} &= 4+1-\frac{1.25\times10^{-4}}{T_s}\\ \frac{1}{60} &= 5T_S - 1.25\times10^{-4}\\ T_s &= \frac{\frac{1}{60}+1.25\times10^{-4}}{5}\\ T_s &= 3.358333\times10^{-3}\ s\\ f_s &= 297.766779\ Hz\end{aligned} \tag{34}$$

Finally, (35) define n for this frequency.

$$n = \frac{f_s}{f_r} = \frac{297.766779}{60} = 4.96278 \tag{35}$$

Given the value of n, the number of cycles p required to achieve accuracy comparable to that of an 8 kHz sampling rate is determined by dividing the total number of samples by n. The objective is to ensure that p is less than or equal to 133 and as close as possible to an integer value.

Consequently, the closest sample count that satisfies this criterion is 129, which results in a value of p that closely approximates an integer. This configuration corresponds to approximately 26 cycles of a 60 Hz signal, as shown in equation (36).

$$p = \frac{129}{4.96278} = 25.993496 \tag{36}$$

In the context of modern power theory measurements, the use of 128 samples per 60 Hz cycle has been considered sufficient to achieve an acceptable level of accuracy (10). This value is approximately equal to the number of samples proposed in this work.

C. Comparison Strategy

Computational simulations were performed in the discrete-time domain for two four-wire systems. The algorithms were implemented using the MATLAB/Simulink platform. An M-file function was developed to acquire data at the specified sampling frequency and to store it in a vector, enabling accurate calculation of the RMS and mean values. The pseudo-codes for these implementations are presented in Algorithms 1 and 2, corresponding to the RMS and mean value calculations, respectively. Subsequent computations were carried out using the formulations described in Section I-A2. It is important to note that sampling at the desired frequency can be achieved in microcontrollers through the use of internal timers. As an example, the Simulink block diagram for calculating the current I_a^b is shown in Figure 3.

The first system consisted of an unbalanced RL load, while the second involved an unbalanced non-linear load. Power calculations for both systems were performed using the CPT method. The simulation carried out at a sampling rate of 297.766779 Hz was compared to a reference simulation conducted in the continuous-time domain. Similarly, simulations at the other sampling rates——15.36 kHz, 7.68 kHz, 1.92 kHz, and 300 Hz——were also compared to the reference case.

Fig. 3. Calculation of i_a^b according to the method described.

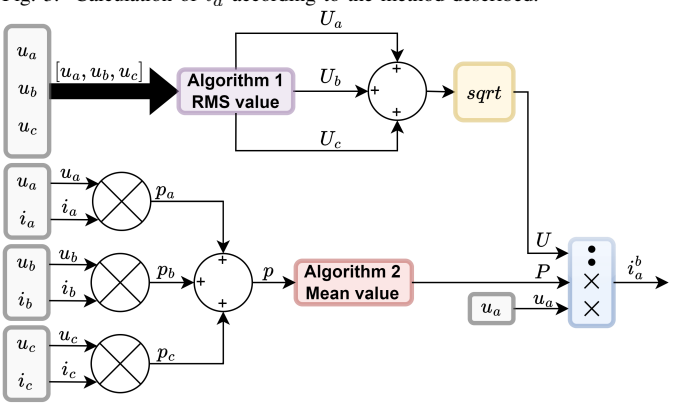

Algorithm 1 RMS calculation after storing 129 samples

Initialize: $s \leftarrow 0$, $i \leftarrow 1$, $m \leftarrow 0$
while 1 **do**
  $s \leftarrow s + u^2$ {Accumulate squared values}
  $i \leftarrow i + 1$ {Increase sample counter}
  if $i = 130$ **then**
    $m \leftarrow \sqrt{s/129}$ {Calculate RMS value}
    $i \leftarrow 1$ {Reset sample counter}
    $s \leftarrow 0$ {Reset accumulator}
  end if
end while=0

*1) **Unbalanced RL circuit**:* A three-phase unbalanced RL circuit comprises RL loads connected to each phase, along with an additional resistive load between phases A and B. The circuit is illustrated in Figure 4, with its parameters listed in Table I. The corresponding voltages and currents are depicted in Figure 5. Voltage measurements were performed between points a, b, and c relative to ground, while current measurements were conducted in series with the power source.

The simulations were conducted using ten different load configurations, which are detailed in Table II.

*2) **Unbalanced non-linear three-phase circuit**:* The unbalanced non-linear three-phase circuit consists of uncontrolled rectifiers supplying RC loads. The circuit schematic is presented in Figure 6, with the corresponding parameters listed in Table III. The measured voltages and currents are depicted in Figure 7, illustrating the behavior of the heavily non-linear

Algorithm 2 Mean calculation after storing 129 samples

Initialize: $s \leftarrow 0$, $i \leftarrow 1$, $m \leftarrow 0$
while 1 **do**
  $s \leftarrow s + u$ {Accumulate summed values}
  $i \leftarrow i + 1$ {Increase sample counter}
  if $i = 130$ **then**
    $m \leftarrow s/129$ {Calculate mean value}
    $i \leftarrow 1$ {Reset sample counter}
    $s \leftarrow 0$ {Reset accumulator}
  end if
end while=0

Fig. 4. Unbalanced RL circuit.

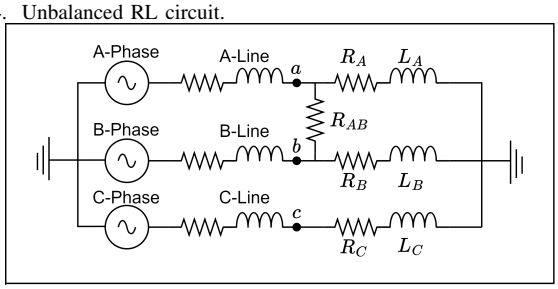

TABLE I
UNBALANCED RL CIRCUIT.

Description	Parameter
A-phase	$127\angle 0$
B-phase	$127\angle -120$
C-phase	$127\angle 120$
A-line	$15m\Omega$ $25\mu H$
B-line	$15m\Omega$ $25\mu H$
C-line	$15m\Omega$ $25\mu H$

TABLE II
UNBALANCED RL CIRCUIT LOADS.

Z_1	Z_2
$R_A = 10\ \Omega$	$R_A = 10/2\ \Omega$
$L_A = 13\ mH$	$L_A = 13/2\ mH$
$R_B = 15\ \Omega$	$R_B = 15/2\ \Omega$
$L_B = 12\ mH$	$L_B = 12/2\ mH$
$R_C = 7\ \Omega$	$R_B = 7/2\ \Omega$
$L_C = 18\ mH$	$L_C = 18/2\ mH$
$R_{AB} = 20\ \Omega$	$R_{AB} = 20/2\ \Omega$
Z_3	Z_4
$R_A = 10/3\ \Omega$	$R_A = 10/4\ \Omega$
$L_A = 13/3\ mH$	$L_A = 13/4\ mH$
$R_B = 15/3\ \Omega$	$R_B = 15/4\ \Omega$
$L_B = 12/3\ mH$	$L_B = 12/4\ mH$
$R_C = 7/3\ \Omega$	$R_B = 7/4\ \Omega$
$L_C = 18/3\ mH$	$L_C = 18/4\ mH$
$R_{AB} = 20/3\ \Omega$	$R_{AB} = 20/4\ \Omega$
Z_5	Z_6
$R_A = 10/5\ \Omega$	$R_A = 10/6\ \Omega$
$L_A = 13/5\ mH$	$L_A = 13/6\ mH$
$R_B = 15/5\ \Omega$	$R_B = 15/6\ \Omega$
$L_B = 12/5\ mH$	$L_B = 12/6\ mH$
$R_C = 7/5\ \Omega$	$R_B = 7/6\ \Omega$
$L_C = 18/5\ mH$	$L_C = 18/6\ mH$
$R_{AB} = 20/5\ \Omega$	$R_{AB} = 20/6\ \Omega$
Z_7	Z_8
$R_A = 10/7\ \Omega$	$R_A = 10/8\ \Omega$
$L_A = 13/7\ mH$	$L_A = 13/8\ mH$
$R_B = 15/7\ \Omega$	$R_B = 15/8\ \Omega$
$L_B = 12/7\ mH$	$L_B = 12/8\ mH$
$R_C = 7/7\ \Omega$	$R_B = 7/8\ \Omega$
$L_C = 18/7\ mH$	$L_C = 18/8\ mH$
$R_{AB} = 20/7\ \Omega$	$R_{AB} = 20/8\ \Omega$
Z_9	Z_{10}
$R_A = 10/9\ \Omega$	$R_A = 10/10\ \Omega$
$L_A = 13/9\ mH$	$L_A = 13/10\ mH$
$R_B = 15/9\ \Omega$	$R_B = 15/10\ \Omega$
$L_B = 12/9\ mH$	$L_B = 12/10\ mH$
$R_C = 7/9\ \Omega$	$R_B = 7/10\ \Omega$
$L_C = 18/9\ mH$	$L_C = 18/10\ mH$
$R_{AB} = 20/9\ \Omega$	$R_{AB} = 20/10\ \Omega$

load system. Voltage measurements were taken between points a, b, and c relative to ground, and current measurements were conducted in series with the power source.

TABLE III
UNBALANCED RL CIRCUIT.

Description	Parameter
A-phase	$127\angle 0°$
B-phase	$127\angle -120°$
C-phase	$127\angle 120°$
A-line	$6\,m\Omega \quad 200\,\mu H$
B-line	$6\,m\Omega \quad 200\,\mu H$
C-line	$6\,m\Omega \quad 200\,\mu H$

Table IV summarizes the parameters of the ten loads simulated in the three-phase unbalanced non-linear circuit.

II. RESULTS

Power measurements were performed in the discrete-time domain at multiple sampling rates, while a reference simulation was conducted in the continuous-time domain. For each of the ten distinct simulations, the percentage error was calculated, followed by the determination of the mean percentage error corresponding to each sampling rate.

A. Unbalanced RL circuit

Initial simulations were conducted on the four-wire unbalanced RL three-phase circuit depicted in Figure 4. Power components were computed following the Conservative Power Theory (CPT).

Table V summarizes the CPT power measurements for the continuous-time reference simulation, while Table VI details the power measurements obtained at a sampling frequency of 297.766779 Hz.

Finally, Table VII summarizes the mean percentage errors computed across all simulations for each respective sampling frequency.

Table VII indicates that only the reactive power (Q) exhibited a mean percentage error exceeding 3.4% at the 297.766779 Hz sampling frequency.

Fig. 5. a) Voltage waveforms for unbalanced RL loads from Z_1. b) Current waveforms for unbalanced RL loads from Z_1.

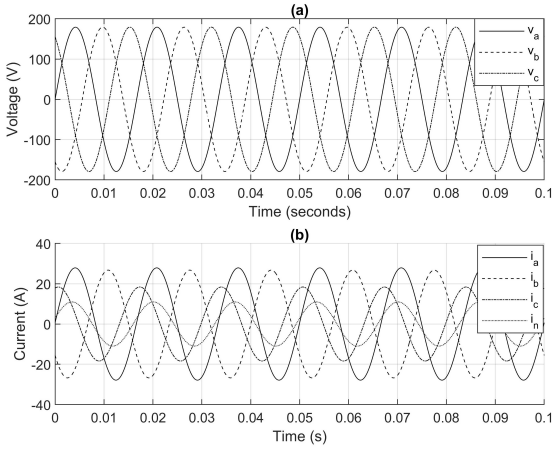

Fig. 6. Unbalanced non-linear three-phase circuit.

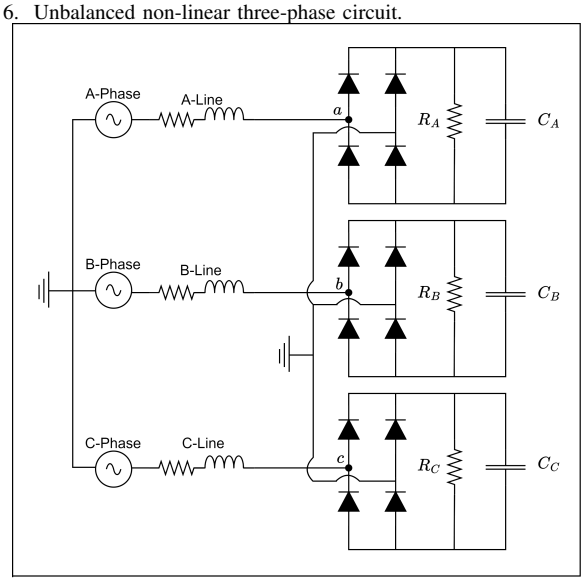

TABLE IV
UNBALANCED NON-LINEAR THREE-PHASE CIRCUIT LOADS.

Z_1	Z_2
$R_A = 1.5\ \Omega$ $C_A = 5.5\ mF$ $R_B = 900\ m\Omega$ $C_B = 2\ mF$ $R_C = 400\ m\Omega$ $C_C = 3.8\ mF$	$R_A = 1.5/2\ \Omega$ $C_A = 5.5\ mF$ $R_B = 900/2\ m\Omega$ $C_B = 2\ mF$ $R_B = 400/2\ m\Omega$ $C_C = 3.8\ mF$
Z_3	Z_4
$R_A = 1.5/3\ \Omega$ $C_A = 5.5\ mF$ $R_B = 900/3\ m\Omega$ $C_B = 2\ mF$ $R_C = 400/3\ m\Omega$ $C_C = 3.8\ mF$	$R_A = 1.5/4\ \Omega$ $C_A = 5.5\ mF$ $R_B = 900/4\ m\Omega$ $C_B = 2\ mF$ $R_B = 400/4\ m\Omega$ $C_C = 3.8\ mF$
Z_5	Z_6
$R_A = 1.5/5\ \Omega$ $C_A = 5.5\ mF$ $R_B = 900/5\ m\Omega$ $C_B = 2\ mF$ $R_C = 400/5\ m\Omega$ $C_C = 3.8\ mF$	$R_A = 1.5/6\ \Omega$ $C_A = 5.5\ mF$ $R_B = 900/6\ m\Omega$ $C_B = 2\ mF$ $R_B = 400/6\ m\Omega$ $C_C = 3.8\ mF$
Z_7	Z_8
$R_A = 1.5/7\ \Omega$ $C_A = 5.5\ mF$ $R_B = 900/7\ m\Omega$ $C_B = 2\ mF$ $R_C = 400/7\ m\Omega$ $C_C = 3.8\ mF$	$R_A = 1.5/8\ \Omega$ $C_A = 5.5\ mF$ $R_B = 900/8\ m\Omega$ $C_B = 2\ mF$ $R_B = 400/8\ m\Omega$ $C_C = 3.8\ mF$
Z_9	Z_{10}
$R_A = 1.5/9\ \Omega$ $C_A = 5.5\ mF$ $R_B = 900/9\ m\Omega$ $C_B = 2\ mF$ $R_C = 400/9\ m\Omega$ $C_C = 3.8\ mF$	$R_A = 1.5/10\ \Omega$ $C_A = 5.5\ mF$ $R_B = 900/10\ m\Omega$ $C_B = 2\ mF$ $R_B = 400/10\ m\Omega$ $C_C = 3.8\ mF$

Fig. 7. a) Voltage waveforms for unbalanced non-linear loads from Z_1. b) Current waveforms for unbalanced non-linear loads from Z_1.

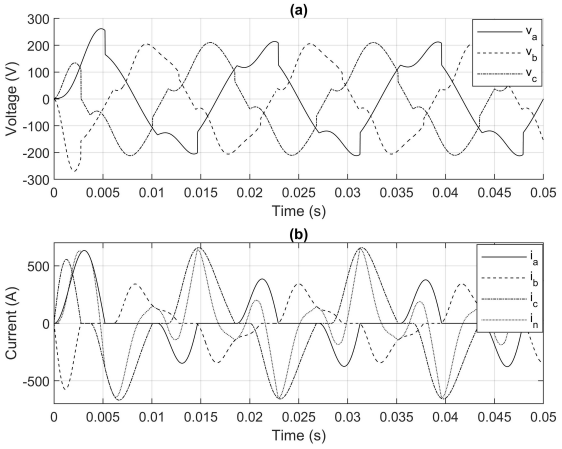

TABLE V
CPT POWER MEASUREMENTS FOR THE REFERENCE SIMULATION.

Loads	P	Q	A	N_a	N_r	N
Z_1	5878	2086	6658	1670	1661	2318
Z_2	11726	4173	13283	3325	3200	4615
Z_3	17545	6259	19874	4967	4777	6891
Z_4	23334	8345	26431	6595	6338	9146
Z_5	29093	10431	32957	8209	7884	11381
Z_6	34824	12517	39449	9809	9415	13596
Z_7	40526	14602	45908	11397	10931	15791
Z_8	46199	16687	52336	12970	12432	17966
Z_9	51843	18771	58732	14531	13918	20122
Z_{10}	57459	20855	65095	16079	15391	22258

TABLE VI
CPT POWER MEASUREMENTS FOR THE 297.766779 HZ SAMPLING SIMULATION.

Loads	P	Q	A	N_a	N_r	N
Z_1	5845	1892	6621	1672	1661	2357
Z_2	11662	3785	13208	3329	3306	4692
Z_3	17447	5678	19762	4974	4937	7008
Z_4	23203	7571	26282	6605	6551	9303
Z_5	28931	9467	32770	8222	8149	11576
Z_6	34631	11361	39227	9827	9733	13831
Z_7	40296	13255	45644	11416	11299	16062
Z_8	45937	15151	52035	12994	12852	18276
Z_9	51550	17050	58396	14562	14391	20473
Z_{10}	57133	18946	64722	16114	15914	22647

TABLE VII
MEAN PERCENTAGE ERRORS – CPT – RL LOAD.

	15.36 kHz ($n = 256$)	7.68 kHz ($n = 128$)	1.92 kHz ($n = 32$)	300 Hz ($n = 5$)	297.766779 Hz ($n = 129$)
P	0.00%	0.01%	0.00%	1.19%	0.56%
Q	3.43%	6.88%	27.81%	17.14%	9.24%
A	0.00%	0.19%	0.00%	0.00%	0.57%
N_a	1.00%	0.98%	0.98%	0.99%	0.17%
N_r	0.99%	1.96%	7.64%	34.35%	3.36%
N	0.99%	1.45%	4.24%	18.17%	1.71%

B. Unbalanced non-linear circuit

The second set of results pertains to the unbalanced non-linear circuit, with power measurements obtained via the Conservative Power Theory (CPT).

Reference power measurements for simulations involving non-linear loads are presented in Table VIII, while Table IX reports the corresponding measurements at a reduced sampling frequency of 297.766779 Hz. Furthermore, Table X summarizes the mean percentage errors observed across the different sampling rates.

TABLE VIII
CPT POWER MEASUREMENTS FOR THE REFERENCE SIMULATION.

Loads	P	Q	A	N_a	N_r	N
Z_1	82709	23760	103104	35383	18182	39781
Z_2	144597	29391	168374	66473	10923	67365
Z_3	190230	34642	220506	95658	8780	96090
Z_4	222292	36549	258001	118020	9237	118381
Z_5	244574	36099	283716	133193	9241	133513
Z_6	259923	34454	300955	142877	8860	143152
Z_7	270357	32497	312248	148725	8359	148960
Z_8	277268	30625	319320	151900	7917	152106
Z_9	281608	28985	323330	153181	7609	153369
Z_{10}	284037	27616	325074	153093	7455	153275

TABLE IX
CPT POWER MEASUREMENTS FOR THE 297.766779 HZ SAMPLING SIMULATION.

Loads	P	Q	A	N_a	N_r	N
Z_1	81654	25429	102007	35311	18995	40096
Z_2	143068	32796	166603	65482	12995	66759
Z_3	188445	38470	218388	94817	10592	95406
Z_4	220455	40979	256043	117080	11438	117637
Z_5	242839	41212	281813	132474	9748	132832
Z_6	258396	39513	299480	142352	9454	142665
Z_7	268996	37029	310432	147521	9132	147803
Z_8	275973	36436	317376	150678	8262	150904
Z_9	280370	34639	321598	151911	8131	152128
Z_{10}	282833	33809	323486	152004	7902	152200

TABLE X
MEAN PERCENTAGE ERRORS – CPT – NON-LINEAR LOAD.

	15.36 kHz ($n = 256$)	7.68 kHz ($n = 128$)	1.92 kHz ($n = 32$)	300 Hz ($n = 5$)	297.766779 Hz ($n = 129$)
P	0.09%	0.09%	0.11%	0.30%	0.73%
Q	8.64%	16.70%	71.69%	374.44%	14.60%
A	0.09%	0.10%	1.23%	0.84%	0.72%
N_a	0.21%	0.27%	0.87%	4.08%	0.74%
N_r	4.56%	12.98%	90.20%	783.89%	10.66%
N	0.16%	0.31%	1.47%	15.38%	0.69%
V	1.25%	10.41%	83.94%	100%	9.32%

Table X indicates that, at the reduced sampling rate, four out of seven measured parameters (P, A, N_a, and N) exhibited errors below 0.8%. Moreover, the mean percentage errors at this sampling rate closely correspond to those observed in the 7.68 kHz simulations, with differences of less than 1.1% for five out of seven parameters.

C. Statistical Analysis

Two hypothesis tests were conducted to evaluate the accuracy and precision of the 297.766779 Hz sampling rate. The first test, the Mann-Whitney test (also known as the Wilcoxon Rank-Sum test) (11), compares mean values of power measurements obtained at the reduced sampling rate against those from the continuous-time domain, thereby assessing accuracy.

The second test, the Brown-Forsythe test (12), evaluates the homogeneity of variances between the samples, providing a measure of precision. Both tests were performed at a significance level of 5%.

1) Mann-Whitney Test: Considering the mean values from the continuous domain and those from the reduced sampling are μ_1 and μ_2, respectively, the null hypothesis and the alternative hypothesis are described in (37) and (38).

The Mann-Whitney test is a non-parametric method used to compare the mean value of populations that do not follow a normal distribution. However, it assumes that the two populations have similar distribution shapes and variances for the test results to be valid.

Let the mean values of the continuous-time domain and reduced sampling populations be denoted by μ_1 and μ_2, respectively. The null hypothesis H_0 and the alternative hypothesis H_1 are stated as follows:

$$H_0 : \mu_1 = \mu_2 \tag{37}$$

$$H_1 : \mu_1 \neq \mu_2 \tag{38}$$

The test procedure consists of ordering the combined samples in ascending order and assigning ranks to each observation based on its position in the ordered list. The sums of ranks for each sample are denoted by R_1 and R_2. These rank sums are subsequently used to compute the test statistics U_1 and U_2, as defined in equations (39) and (40).

$$U_1 = N_1 \times N_2 + \frac{N_1(N_1+1)}{2} - R_1 \tag{39}$$

$$U_2 = N_1 \times N_2 + \frac{N_2(N_2+1)}{2} - R_2 \tag{40}$$

Where:

N_1: number of elements in the first group.

N_2: number of elements in the second group.

Finally, the smaller value between U_1 and U_2 is selected and compared against the critical value from the Mann-Whitney distribution table at the specified significance level. If the calculated value is less than or equal to the critical value, the null hypothesis is rejected. Otherwise, the null hypothesis cannot be rejected, implying that there is insufficient evidence to conclude that the populations represented by the samples differ in their mean values.

For a significance level α = 0.05, two groups of samples were compared, each containing 20 elements for all power components (10 from RL load simulations and 10 from non-linear load simulations), except for the void power measurements which only appear in non-linear load simulations. The critical values used were 127 for samples of size 20 and 23 for void power measurements. The Mann-Whitney test statistics for all CPT-measured power components are summarized in Table XI.

TABLE XI
U CALCULATED VALUE FOR THE POWER MEASUREMENTS OF CPT.

	P	Q	A	N_a	N_r	N	V
U	190	177	190	199	169	200	41

From Table XI it is observed that all minimum values between U_1 and U_2 are smaller than the corresponding critical values. Therefore, the null hypothesis — which states that the mean values of the populations in the continuous-time domain and at the 297.766779 Hz sampling rate are equal — cannot be rejected.

Additionally, these data allow the calculation of a Z statistic, which can be compared to the critical Z value as a complementary validation of the previous test results. To compute Z, the observed U, denoted as $U_{observed}$, is designated as the maximum value between U_1 and U_2, while the expected value $U_{expected}$ is defined as the mean of U_1 and U_2. The standard error of U is then calculated as shown in (41).

$$U_{StdError} = \sqrt{\frac{(N_1 \times N_2(N_1+N_2+1)}{12}} \tag{41}$$

The value of Z is computed as shown in equation 42, and the critical value of Z for $\alpha = 0.05$, considering a two-tailed test, is 1.96. If the critical value of Z is bigger than the calculated one, it is not possible to reject the null hypothesis.

$$Z = \frac{U_{observed} - U_{expected}}{U_{StdError}} \tag{42}$$

Table XII presents the computed Z values for each of the power measurements.

TABLE XII
Z VALUES FOR Z ON MANN-WHITNEY TEST.

	P	Q	A	N_a	N_r	N
$U_{observed}$	210	223	210	201	231	200
$U_{expected}$	200	200	200	200	231	200
$U_{StdError}$	36.97	36.97	36.97	36.97	36.97	36.97
Z	0.27	0.62	0.27	0.03	0.84	0

According to the data, the results of the Z-test are consistent with those of the Mann-Whitney test, confirming that the null hypothesis cannot be rejected.

2) Brown-Forsythe Test: The Brown-Forsythe test is a non-parametric test derived from the Levene test. It utilizes the median instead of the mean to enhance the robustness of the results against non-normal data distributions. Considering the standard deviations from the continuous domain and those from the reduced sampling are σ_1^2 and σ_2^2, respectively, the null hypothesis and the alternative hypothesis are formulated in (43) and (44).

$$H_0 : \sigma_1^2 = \sigma_2^2 \tag{43}$$

$$H_1 : \sigma_1^2 \neq \sigma_2^2 \tag{44}$$

The test consists of calculating the W parameter, as in (45):

$$W = \frac{\frac{\sum_{i=1}^{k} N_i (Z_{i.} - Z_{..})^2}{K-1}}{\frac{\sum_{i=1}^{k} \sum_{j=1}^{N_i} (Z_{ij} - Z_{i.})^2}{(N-K)}} \tag{45}$$

Where:
k: number of groups of samples.
N_i: number of elements of the $i^{th} sample$.
N: number of elements of all samples.
Y_{ij}: Value of the i^{th} element of the i^{th} sample.
$Z_{ij} = \left| Y_{ij} - \tilde{Y}_i \right|$: $\tilde{Y}_i$ is the median of the i^{th} sample.

The null hypothesis is rejected if W exceeds the critical value of distribution F, determined at the chosen significance level, with (K-1) and (N-K) degrees of freedom. Specifically, the degrees of freedom are 1 and 38 for all power measurements, except for the void power measurement, where the degrees of freedom are 1 and 18, respectively.

The level of significance and sample sizes used in this test are the same as those employed in the Mann-Whitney test. The statistical results for all power measurements are presented in Table XIII.

TABLE XIII
U CALCULATED VALUE FOR POWER MEASUREMENTS.

	P	Q	A	N_a	N_r	N	V
W	0.00	2.88	0.00	0.00	0.12	0.00	0.62

Considering that the critical values of the F distribution are 4.098 for all power measurements and 4.414 for the void power measurement, the null hypothesis cannot be rejected based on this criterion.

D. Increasing samples for measuring

It is possible to maintain the same reduced frequency while utilizing a greater number of sample points to decrease the error between the reference measurements and those at the reduced sampling rate. However, this approach comes at the cost of increased computational time, as more 60 Hz cycles are required to form a larger sample vector.

The initial proposal employed an 8 kHz sampling frequency, which corresponds to 133 sample points within a 60 Hz cycle. To explore the impact of a denser sample vector, the number of samples corresponding to a 16 kHz frequency within a 60 Hz cycle, namely 256 samples, was used for comparison.

The procedure described from (30) to (35) was retained. The only modification occurred in (36), where the number of samples was adjusted to be equal to or less than 256, ensuring that the resulting ratio approximates an integer as closely as possible. Consequently, 254 samples were determined to be suitable.

New simulations were conducted, and Table XIV presents the mean errors for the reduced sampling frequencies, comparing results for n = 129 and n = 254 with the reference data for both RL and non-linear loads.

TABLE XIV
MEAN ERROR WITH REDUCED SAMPLING FREQUENCY FOR DIFFERENTE SAMPLE POINTS.

	RL		Non-linear	
	n=129	n=254	n=129	n=254
P	0.56%	0.33%	0.73%	0.33%
Q	9.24%	3.57%	14.6%	5.92%
A	0.57%	0.30%	0.72%	0.35%
N_a	0.17%	0.91%	0.74%	0.47%
N_r	3.36%	0.29%	10.66%	5.54%
N	1.71%	0.62%	0.69%	0.38%
V			9.32%	2.01%

As anticipated, increasing the number of sample points while maintaining the same reduced sampling frequency substantially decreases the errors associated with measuring and calculating CPT power components.

This approach enables the designer to adjust the number of samples to achieve the permissible error level for a specific application.

III. CONCLUSION

In this paper, the reduced sampling frequency contributes to lowering computational costs while enhancing noise immunity. The employed method demonstrated the feasibility of achieving these goals with acceptable levels of accuracy and precision.

For the RL unbalanced circuits with n = 129 samples, errors in five out of six power measurements were below 1.8%, with the remaining measurement errors ranging between 3.4% and 9.3%. In the non-linear circuit, four out of seven measurements had errors under 1.0%, while the others ranged up to 9.4%, 10.7%, and 14.6%. The largest errors occurred in the measurements of Q, N_r, and V, especially under heavy non-linear load conditions.

Considering n = 254 samples, the RL unbalanced circuit results showed that six out of seven power measurements exhibited errors below 1.0%, with the remaining measurement below 3.6%. For the non-linear circuit, four out of seven measurements had errors of less than 0.5%, and the others were below 2.01%, 5.54%, and 5.92%. The most significant errors remained in the same power components but were reduced by factors of two to five compared to the n = 129 sample scenario.

An additional noteworthy observation is that the errors from measurements with reduced sampling at n = 129 samples were comparable to those at 7.68 kHz, while those at n = 254 samples were comparable to 15.36 kHz. This comparison is significant because the 7.68 kHz and 15.36 kHz sampling rates correspond to 128 and 256 samples per cycle, respectively. Remarkably, ten out of thirteen measurements—across both RL unbalanced and non-linear loads—exhibited error differences of less than 1.5% between the 7.68 kHz and 297.766779 Hz with n = 129 samples, with the remaining three differences below 2.5%. Regarding the 15.36 kHz and 297.766779 Hz with n = 254 samples, twelve out of thirteen measurements differed by less than 1.0%.

Finally, the Mann-Whitney and Brown-Forsythe hypothesis tests were employed to compare the means and variances, respectively, between the continuous domain and reduced sampling data. Both tests supported the null hypothesis, indicating no significant difference in mean or variance between the two sampling frequencies. This study thus opens possibilities and discussions regarding power measurements at low sampling frequencies, achieving results comparable to those obtained with higher-frequency data acquisition systems.

It is important to emphasize that the focus of this novel methodology is not on minimizing the time delay required to reach steady-state values. Instead, it prioritizes a cost-effective approach that enables accurate power measurements on low-cost microcontrollers, making it a practical and accessible solution.

ACKNOWLEDGMENT

The authors would like to thanks UFMS, the PPGEE-UFMS, CNPq (Process 306749/2022-0) and CAPES (Finance Code 001).

REFERENCES

[1] P. Tenti, H. K. M. Paredes, F. P. Marafao, and P. Mattavelli, "Accountability in smart microgrids based on conservative power theory. ieee transactions on instrumentation and measurement." *IEEE Transactions on Instrumentation and Measurement*, vol. 60, no. 9, pp. 3058–3069, 2011.

[2] S. Yang, K. W. Lao, H. Hui, Y. Chen, and N. Dai, "Real-time harmonic contribution evaluation considering multiple dynamic customers." *CSEE Journal of Power and Energy Systems.*, pp. 1–13, 2023.

[3] S. Svensson, "Power measurement techniques for non-sinusoidal conditions: The significance of harmonics for the measurement of power and other ac quantities." Ph.D. dissertation, Chalmers University of Technology, 1999.

[4] S. M. Salam, M. I. Uddin, and M. R. B. Moinuddin, "Impact analysis of large number of non-linear lighting loads on power quality in distribution network," 2019, paper presented at the 4th international conference on electrical information and communication technology. Khulna, Bangladesh 20–22 Dec 2019.

[5] M. A. G. de Brito, M. G. Alves, and C. A. Canesin, "Hybrid mppt solution for double-stage photovoltaic inverter." *Journal of Control, Automation and Electrical Systems.*, vol. 30, pp. 253–265, 2019.

[6] M. A. de Brito, A. S. Volpato, E. A. Batista, and R. B. Godoy, "Power electronics converters for an electric charging station: Description and experimental evaluation." *Transportation Research Procedia.*, vol. 70, pp. 154–161, 2023.

[7] N. D. de Andrade, R. B. Godoy, E. A. Batista, M. A. de Brito, and R. L. Soares, "Embedded fpga controllers for current compensation based on modern power theories." *Energies.*, vol. 15, no. 17, p. 6284, 2022.

[8] L. R. Souza, R. B. Godoy, M. A. de Souza, L. G. Junior, and M. A. de Brito, "Sampling rate impact on electrical power measurements based on conservative power theory." *Energies.*, vol. 14, no. 19, p. 6285, 2021.

[9] P. Tenti, H. K. M. Paredes, and P. Mattavelli, "Conservative power theory, a framework to approach control and accountability issues in smart microgrids." *IEEE Transactions on Power Electronics.*, vol. 26, no. 3, pp. 664–673, 2010.

[10] J. C. Alfonso-Gil, S. Orts-Grau, N. Munoz-Galeano, F. J. Gimeno-Sales, and S. Segui-Chilet, "Measurement system for a power quality improvement structure based on ieee std. 1459." *IEEE Transactions on Power Electronics*, vol. 62, no. 12, pp. 3177–3188, 2013.

[11] T. W. MacFarland and J. M. Yates, "Mann–whitney u test," in *Introduction to Nonparametric Statistics for the Biological Sciences Using R*. Cham: Springer International Publishing, 2016, pp. 103–132.

[12] M. B. Brown and A. B. Forsythe, "Robust tests for the equality of variances." *Journal of the American Statistical Association.*, vol. 69, no. 346, pp. 364–367, 1974.

Victor A. de A. Prado holds a Master's degree in Electrical Engineering from the Federal University of Mato Grosso do Sul (UFMS), obtained in 2021. His dissertation was titled "Power Measurements According to the Conservative Power Theory (CPT) and IEEE 1459-2010 Implemented with Reduced Sampling Rate." He received his Bachelor's degree in Electrical Engineering from UFMS in 2018, with a thesis titled "Comparative Study of PLL Algorithms Applied to Synchronization of Distributed Generation Systems with the Power Grid."

Nicholas D. Delben is currently pursuing a Ph.D. in Electrical Engineering at the Federal University of Rio de Janeiro (UFRJ). He holds a Master's degree in Electrical Engineering from the Federal University of Mato Grosso do Sul (UFMS), with an emphasis on Power Systems and a dissertation focused on Parallel Active Power Filters for Improving Power Quality. He participated in the Tutorial Education Program and the V2G-UFMS research project. His research interests include power electronics, power quality, smart grids, wireless power transfer for electric vehicle applications, and the application of active filters for power factor enhancement.

Ianca M. S. de Jesus received the degree in Electrical Engineering from the Federal University of Mato Grosso do Sul (UFMS). She is currently pursuing a master's degree in Electronic Energy Processing at UFMS. She serves as the President of the IEEE Power Electronics Society (PELS) chapter at UFMS. Her research experience includes participation in projects on bidirectional wireless energy transfer for Vehicle-to-Grid (V2G) applications, liquefied petroleum gas (LPG) as an energy resource in aquaculture, wireless charging for implantable devices, and advanced materials electrochemistry. She has also been involved in the Electrical Engineering Tutorial Education Program (PET-Elétrica) at UFMS.

Ruben B. Godoy holds a Ph.D. in Electrical Engineering from São Paulo State University (UNESP, 2010) and completed a postdoctoral fellowship at École de Technologie Supérieure (ÉTS), Canada (2014). He is an Associate Professor IV at the Federal University of Mato Grosso do Sul (UFMS), fully dedicated to teaching, research, and innovation in power electronics, electric vehicle charging systems, wireless power transfer, and smart inverters. He authored the technical book Wireless Power Transfer: Classic Topologies for Inductive Coupling (Appris, 2024) and has published in high-impact journals like IEEE Transactions on Power Electronics. He also coordinates extension projects, such as photovoltaic water pumping in Guinea-Bissau, combining technology with social impact. His work has been recognized by awards like the Best Educational Impact Award (IEEE, 2015) and the Outstanding Innovation Award (IEEE, 2011).

Edson A. Batista holds a degree in Electrical Engineering (2001), a master's (2004), and a Ph.D. (2009) in Electrical Engineering from São Paulo State University (UNESP/FEIS). He completed a postdoctoral fellowship at the University of Tennessee's Department of Nuclear Engineering (2015-2016). He is currently an Associate Professor at FAENG/UFMS, Coordinator of the Graduate Program in Electrical Engineering, and leader of the Embedded Systems Laboratory. He has coordinated projects funded by agencies like CNPq and FUNDECT/MS and supervised the EngeFour Junior Enterprise. His research interests include Smart Grid, IoT, Electric Mobility, intelligent instrumentation (IEEE 1451), real-time HIL simulation, fractional calculus-based controllers, and model predictive control. In 2021, he was recognized as an Outstanding Researcher by the Government of Mato Grosso do Sul. He also coordinates an international dual-degree program with the Polytechnic Institute of Bragança (Portugal) and CeDRI. He co-founded two startups: ENG Tecnologia Ltda., focused on IoT solutions, and DAMINE, which applies AI to image processing for decision-making.

Moacyr A. G. de Brito holds a Bachelor's degree in Electrical Engineering from São Paulo State University (UNESP), Ilha Solteira campus (2005), and earned his Master's (2008) and Ph.D. (2013) in Electrical Engineering, specializing in Power Electronics Automation. His doctoral thesis was awarded the best thesis in the Electrical Engineering Graduate Program in 2013. He served as Course Coordinator and held membership positions in academic councils at the Federal University of Technology – Paraná (UTFPR). From 2013 to 2016, he was a professor in the Electronic Engineering program at UTFPR, Campo Mourão campus. Since 2016, he has been a professor in the Electrical Engineering program at the Federal University of Mato Grosso do Sul (UFMS), affiliated with the Artificial Intelligence, Power Electronics, and Digital Electronics Laboratory (BATLAB). He is a permanent professor in the UFMS Graduate Program in Electrical Engineering and a collaborating professor in the doctoral program at the Federal University of Uberlândia (UFU). He acts as a reviewer for several international journals. His research interests include active power factor correction, DC-DC converters, switched-mode power supplies, digital control, FPGAs, isolated and grid-connected inverters using renewable energy sources. He is currently a CNPq research productivity fellow (PQ-2).